Journal of Alloys and Compounds 780 (2019) 90–97

Contents lists available at ScienceDirect

Journal of Alloys and Compounds

journal homepage: http://www.elsevier.com/locate/jalcom

Enhanced electrochemical performance for EDLC using ordered mesoporous carbons (CMK-3 and CMK-8): Role of mesopores and mesopore structures

Tuan Ngoc Phan, Min Kyung Gong, Ranjith Thangavel, Yun Sung Lee**, Chang Hyun Ko*

School of Chemical Engineering, Chonnam National University, Gwangju 61186, Republic of Korea

ARTICLE INFO

Article history:
Received 6 September 2018
Received in revised form
24 November 2018
Accepted 26 November 2018
Available online 27 November 2018

Keywords:
Ordered mesoporous carbon
CMK-3
CMK-8
Mesoporous materials
EDLCs

ABSTRACT

Non-aqueous electrical double-layer capacitors (EDLCs) with high energy density and long cycle life are the key to meet future energy demands. The performance of such high-energy supercapacitors greatly depends on the textural properties of the porous carbon electrode. Ordered mesoporous carbon materials are always the prominent electrodes for capacitor applications and the roles of pore size and pore structure need to be investigated in a non-aqueous capacitor system to achieve high performance. Herein, a series of well-ordered mesoporous carbon materials (OMCs) with high specific surface areas and high pore volumes are synthesized utilizing mesoporous silica (SBA-15 and KIT-6) templates at different carbonization temperatures and studied for EDLCs with non-aqueous electrolytes. The performance of EDLCs greatly depends on the mesopore structure and mesoporous surface area, which is evident from the electrochemical performance. In particular, CMK-3 (prepared using SBA-15) shows a higher specific capacitance than CMK-8 (prepared using KIT-6), which may come from the long straight channels of CMK-3 leading to a lower internal resistance and larger number of ion-diffusion pathways. The mesopores provide not only larger pores for fast electrolyte ion transport but also a high surface area and high pore volume for ion storage during the charge–discharge processes. Increasing the carbonization temperature from 600 to 900 °C increases the mesoporous surface area, resulting in enhanced specific capacitance.

1. Introduction

Increasing energy demands lead to the development of advanced electrochemical energy-storage systems with high performance at low cost [1,2]. Several energy-storage devices, such as lithium-ion batteries, lithium–sulfur batteries, and sodium-ion batteries, have been intensively investigated for future applications [3–5]. However, the sluggish intercalation battery kinetics warrants the need for a device that can deliver high power. Supercapacitors have been attaining greater interest as a potential alternative in applications where batteries fail to deliver high power [6]. Depending on the working mechanism, supercapacitors are classified as (i) electric double-layer capacitors (EDLCs) and (ii) pseudocapacitors. Among these, EDLCs are always of great interest among researchers because of their simple construction, superior power density, excellent reversibility, and good cyclic stability [7,8]. EDLCs store energy by a simple electric double-layer formation at the electrode–electrolyte interface when a potential is introduced between two symmetrical carbon electrodes [9,10].

Unlike pseudocapacitors that work on faradic redox reactions, EDLCs have an extraordinary life expectancy (100,000 cycles). Yet, EDLCs show an unsatisfactory energy output when employed in aqueous electrolytes due to the small working potential (1–1.2 V). This opens the research for development of high-energy EDLCs utilizing non-aqueous organic electrolytes in a wide operating potential window (2.5–3 V) [8,11,12]. However, the performance of EDLCs employing non-aqueous electrolytes suffers from insufficient power and cycle life due to the presence of large solvated ions and the viscous nature of the non-aqueous electrolyte [8,13]. To obtain excellent EDLC performance, the porous electrode materials should have favorable textural properties that enable easy penetration of electrolyte ions into deeper pores for double-layer formation.

* Corresponding author.
** Corresponding author.
E-mail addresses: leeys@jnu.ac.kr (Y.S. Lee), chko@jnu.ac.kr (C.H. Ko).

https://doi.org/10.1016/j.jallcom.2018.11.348
0925-8388/

Porous carbon materials with large surface area, high electrical conductivity, and good chemical stability have been widely investigated as electrode materials for EDLCs [14,15]. In particular, activated carbon from coal and coke was widely studied for aqueous EDLCs and high performance has been achieved. However, activated carbon underperforms when employed in non-aqueous EDLCs because of its highly microporous nature, causing severe ion-diffusional losses at high current densities [16–18]. Graphene, a unique 2-dimensional material with a high surface area ($2600\ m^2\ g^{-1}$) and ultra-high electrical conductivity was studied for EDLC as an alternative to microporous activated carbon [19,20]. The aggregation and re-stacking of the graphene structure during the charge–discharge process inhibits the contact between electrolyte molecules and the graphene surface, consequently reducing the capacitance of graphene-based EDLCs. Various forms of carbon with wider pore sizes have been extensively studied, including carbon nanofibers, carbon nanotubes, onion-like carbon, zeolite template carbon, and carbide-derived carbon [21–25]. However, the poor pore size/shape control and tedious manufacturing process impedes practical application.

In recent years, ordered mesoporous carbons (OMCs) with highly ordered porous structures have been gaining attention for high-performance EDLCs [17,19,26,27]. A combination of a high specific surface area, ordered mesoporous structure, wide pore volume, and easy pore size/shape-tailoring process makes them an emerging alternative for application in EDLCs. The presence of ordered mesopores in a wide size range can facilitate easy contact between the pore wall and electrolyte ions to overcome the diffusion losses with non-aqueous electrolytes [28]. Employing a perfectly engineered mesoporous carbon in non-aqueous EDLCs can achieve a remarkable specific capacitance even at high current densities. However, the dependence of such pore size and shape on the electrochemical performance has not yet been studied for high-energy EDLCs in a non-aqueous medium.

Herein, we synthesize OMCs using two different kinds of mesoporous silica templates and investigate the pore size–structure correlation in high-voltage, non-aqueous EDLCs. The textural characteristics of the mesoporous carbon depends especially on type of template, and carbonization temperature. OMCs CMK-3 were synthesized using a 2D hexagonal SBA-15 template and OMCs CMK-8 were prepared using 3D cubic KIT-6. The obtained OMCs showed a high specific surface area ($>900\ m^2\ g^{-1}$), and large pore volume, delivering excellent specific capacitance compared to microporous carbon materials with low specific surface areas ($145–265\ m^2\ g^{-1}$) in non-aqueous EDLCs. Adjusting the carbonization temperature on CMK-3 and CMK-8 can greatly modify the textural properties of OMCs, such as the mesoporous surface area and pore diameter, leading to a different EDLC performance. The current research provides a platform for developing high-performance EDLCs utilizing perfectly engineered OMCs.

2. Experiment

2.1. Synthesis of mesoporous silica templates

The mesoporous silica templates (SBA-15 and KIT-6) were synthesized according to the procedures reported elsewhere [29]. To synthesize the SBA-15 template, 8.0 g of tri-block copolymer P123 (Sigma-Aldrich) was dissolved in the mixed solution of 60 g distilled water (DW) and 320 g 2 M HCl (Daejung Chemical & Metal, South Korea). After that, 17 g tetraethyl orthosilicate (TEOS, Sigma-Aldrich) was added. The mixture was kept at 35 °C for 20 h and then at 100 °C for 24 h. The white precipitates were collected, washed, dried at 100 °C, and calcined at 550 °C for 2.5 h.

The KIT-6 template was fabricated by first dissolving 9.6 g P123 into 346.6 g DW and 18.8 g concentrated HCl. Then, 9.6 g butanol (Sigma-Aldrich) and 24.8 g TEOS were sequentially added into the above solution. The mixed solution was placed in oven at 35 °C for 24 h and at 100 °C for another 24 h. After filtration and washing, the white powder was finally calcined at 550 °C for 2.5 h.

2.2. Synthesis of CMK-3 and CMK-8

The OMCs (CMK-3 and CMK-8) were prepared by an incipient wetness method using mesoporous silica templates (SBA-15 and KIT-6, respectively), as described in our previous research [26]. Furfuryl alcohol (FA) was used as a carbon source. Typically, 0.8 mL of FA is impregnated into 1.0 g of mesoporous silica templates, followed by drying at 100 °C for 6 h. The samples were treated at 350 °C for 2 h in a N_2 environment with a heating rate of 1.25 °C min^{-1}. Afterward, the second and third impregnation steps were performed with 0.5 mL and 0.2 mL of FA, respectively. After the impregnation processes, the mixed powders were carbonized at high temperatures of 600, 750, and 900 °C for 2 h in a N_2 environment. The carbon-silica samples obtained after carbonization were treated with 50 mL of 2 M NaOH solution and distilled water in order to remove the mesoporous silica templates. The pure OMCs were collected after drying at 100 °C for 12 h. The OMCs synthesized from SBA-15 and KIT-6 are henceforth denoted as CMK-3-*x* and CMK-8-*x*, respectively, where *x* is the carbonization temperature ($x = 600$, 750, and 900).

In order to evaluate the effect of mesoporous structures on the electrochemical performance of OMCs, a series of microporous carbons were prepared by directly carbonizing FA at 600, 750, and 900 °C in N_2 flow without a mesoporous silica template. The obtained carbon samples are denoted as MC-*x* (MC-600, MC-750, and MC-900, respectively).

2.3. Material characterization

N_2 adsorption–desorption experiments were conducted at −196 °C using the TriStar II 3020 system (Micromeritics, USA). Before measurements, the samples were degassed at 100 °C for 24 h. The specific surface area was calculated by the multipoint Brunauer–Emmett–Teller model (S_{BET}, $P/P_0 = 0–0.99$). The total pore volume (V_{tot}) was determined at $P/P_0 = 0.99$. The external surface area (S_{ext}) and the mesoporous surface area (S_{meso}) were estimated by *t-plot* method. Low-angle and high-angle X-ray diffraction (XRD) patterns were obtained using Rigaku D-MAX 3 equipment with Cu Kα radiation at 40 kV and 40 mV. Transmission electron microscopy (TEM) and high-resolution transmission electron microscopy (HR-TEM) images were collected on a CM200 (Philip) system. Raman measurements were performed on a Lab-Ram HR800 instrument (Horiba Jobin-Yvon, installed at Korea Basic Science Institute).

2.4. Preparation of EDLCs and electrochemical measurement

The electrodes for EDLCs were fabricated by accurately weighing the amounts of active material (72 wt%), Ketjen black (14 wt%) as conductive carbon, and Teflonized acetylene black (14 wt%) as binder. The electrode slurry was pressed over a stainless steel mesh and dried at 160 °C for 4 h in a vacuum oven. The mass loading of the EDLCs were ~ 5–6 mg cm^{-2}. EDLCs were assembled in a standard CR2032 coin cell with a symmetrical electrode configuration inside an argon-filled glove box. The electrodes were separated by a porous polypropylene separator (Celgard 3401) and filled with $NaClO_4$ in ethylene carbonate:dimethyl carbonate (1:1 vol/vol). Cyclic voltammetry (CV) and electrochemical impedance spectroscopy (EIS) studies were performed with Bio-Logic (SP-150,

France) electrochemical workstation. Galvanostatic charge/discharge studies were carried between 0 and 3 V at different current densities using a Won-A-Tech WBCS 3000 battery cycler. The current densities are based on the total mass of both electrodes and the specific capacitance is calculated as follows: $Cs\,(\mathrm{F\,g^{-1}}) = 4(I \times t)/(V \times m)$, where I is the applied current (A), t is the discharge time (s), V is the operating voltage (V), and m is the total active mass of the electrode (g).

3. Results & discussion

3.1. Characterization of OMCs

A series of OMCs were fabricated with two kinds of mesoporous silica templates (SBA-15 and KIT-6) at different carbonization temperatures (600, 750, and 900 °C). In the low-angle XRD patterns shown in Fig. 1(a), the CMK-3-*x* samples exhibit a well-resolved peak corresponding to (100) diffraction of the 2D hexagonal space group (*p6mm*) [30]. On the other hand, the CMK-8-*x* samples show a main peak indexed as the (211) diffractions of a cubic *Ia3d* structure [31]. These indicate that CMK-3-*x* and CMK-8-*x* successfully replicated the ordered mesoporous structures of the SBA-15 and KIT-6 templates, respectively. When the carbonization temperature was increased from 600 °C to 900 °C, the intensities of the main peak in the patterns of CMK-3-*x* and CMK-8-*x* increased. This demonstrates that a higher carbonization temperature can form a mesoporous structure with a higher order. In addition, a peak at $2\theta = 23°$ in the high-angle XRD patterns of OMCs (Fig. S1) points out that the obtained OMCs are amorphous materials.

N_2 adsorption–desorption isotherms were obtained to identify the pore structures of the OMCs. Fig. 1(b) shows that all OMCs samples exhibit type-IV isotherms with small H2 hysteresis loops in the relative pressure range between 0.4 and 0.9, indicating the existence of well-ordered mesopores in these OMCs [32,33]. The type-H2 hysteresis loop shows that the mesopores of OMCs are ink-bottle-like mesopores. The pore-size-distribution curves (Fig. S2) of the OMCs, determined using the Barrett–Joyner–Halenda (BJH) method, show narrow peaks with average pore sizes of 3.0–5.0 nm. The detailed textural properties of the silica templates and OMCs are summarized in Table 1. The investigated OMCs exhibit a high specific surface area (approximately 900–1000 $\mathrm{m^2\,g^{-1}}$). The *t-plots* of CMK-3-*x* and CMK-8-*x* (Fig. S3) indicate that the pore structure of these materials contain only mesopores (no micropores) [34]. Thus, the mesoporous surface area can be calculated by subtracting the external surface areas from the total specific surface area. The mesoporous surface area and the average pore size of CMK-3-*x* and CMK-8-*x* increase with increasing the carbonization temperature. Therefore, the carbonization temperature plays an important role in determining the mesopore behavior of OMCs.

In contrast to the mesoporous materials, the MC-*x* samples show type-I N_2 adsorption–desorption isotherms (Fig. S4), indicating only the formation of micropores [33]. MC-*x* materials present a low specific surface area (145–265 $\mathrm{m^2\,g^{-1}}$) and low pore volume (~0.1 $\mathrm{cm^3\,g^{-1}}$), which can lead to poor performance in EDLC tests.

The degree of graphitization of the OMCs was characterized by Raman spectroscopy. The Raman spectra of the OMCs in Fig. S5 exhibit two distinct peaks at approximately 1340 and 1580 $\mathrm{cm^{-1}}$, which are attributed to the D band and G band of carbon materials [35]. The D band is caused by defects and disorders of the six-fold sp^2-hybridized carbon rings, whereas the G band is caused by bond stretching of sp^2 carbon in either rings or chains. The ratio between the peak intensities of the D and G bands (I_D/I_G, Table 1) is commonly used to evaluate the level of graphitization [36,37]. The I_D/I_G values were lowest at 0.75 and 0.78 for CMK-3-750 and CMK-8-750, respectively. This indicates that carbonization at 750 °C can form carbon materials with the highest-ordered graphitic structure. Whereas, CMK-3-900 and CMK-8-900 showed highest I_D/I_G values (0.97 and 0.96, respectively), indicating the lowest degree of graphitization.

Fig. 2 displays the TEM images of CMK-3-*x* and CMK-8-*x* carbonized at different temperatures. The HR-TEM images are displayed in Fig. S6. The CMK-3-*x* samples exhibit long ordered parallel channels, which is the typical 2D hexagonal symmetrical structure (*p6mm*) of mesoporous SBA-15. In the other hand, the CMK-8-*x* samples show the clear *Ia3d* cubic channels of mesoporous KIT-6. These behaviors point out the successful replication of the mesoporous structure of the SBA-15 and KIT-6 templates in

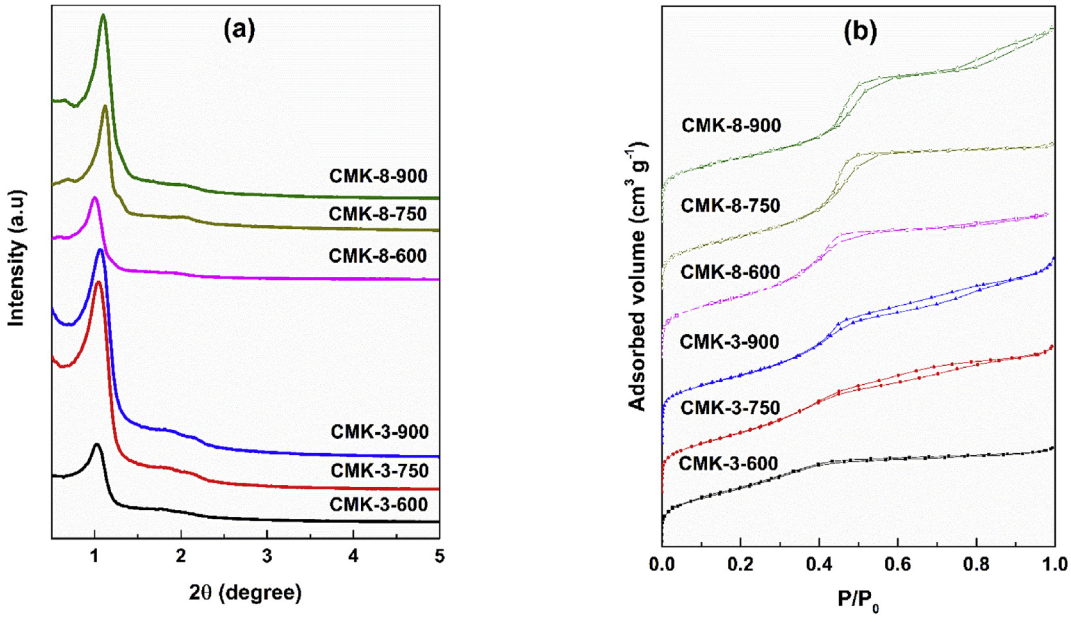

Fig. 1. (a) Low-angle XRD patterns of OMCs and (b) N_2 adsorption–desorption isotherms of OMCs.

Table 1
Textural properties of the mesoporous templates and OMCs.

Samples	S_{BET} ($m^2\ g^{-1}$)	V_{tot} ($cm^3\ g^{-1}$)	Average pore size (nm)[a]	t-plot			I_D/I_G
				S_{meso} ($m^2\ g^{-1}$)	S_{micro} ($m^2\ g^{-1}$)	S_{ext} ($m^2\ g^{-1}$)	
SBA-15	752.3	1.0	5.2	–	–	–	–
CMK-3-600	859.7	0.62	2.9	637.7	0	140	0.82
CMK-3-750	950.6	0.94	4.0	825.2	0	56.3	0.75
CMK-3-900	1064	1.16	4.4	971.8	0	87.7	0.97
KIT-6	743	1.0	5.8	–	–	–	–
CMK-8-600	977.1	0.94	3.9	710.8	0	219	0.88
CMK-8-750	944.2	0.98	4.2	892.0	0	24.9	0.78
CMK-8-900	978.6	1.25	5.1	996.5	0	70.1	0.96
MC-600	264.6	0.14	2.2	–	218.8	45.7	0.71
MC-750	241.8	0.14	2.7	–	182.6	59.2	0.88
MC-900	145.2	0.09	2.7	–	65.9	79.3	0.87

[a] Average pore size calculated by $4V_{tot}/S_{BET}$.

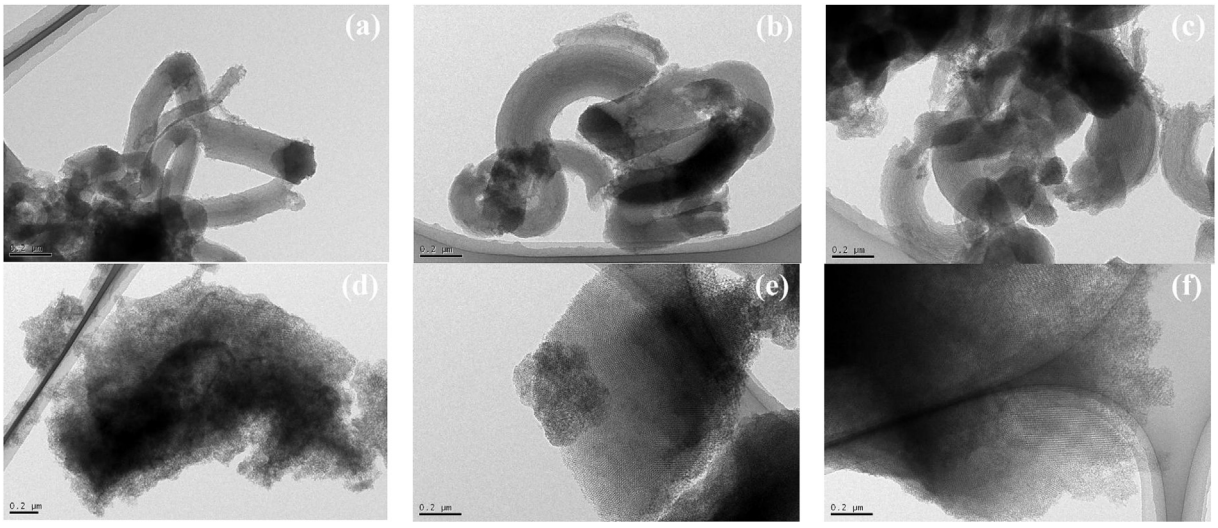

Fig. 2. TEM images of (a) CMK-3-600, (b) CMK-3-750, (c) CMK-3-900, (d) CMK-8-600, (e) CMK-8-750, and (f) CMK-8-900.

the investigated carbon materials. However, there is a small portion of disordered carbon in these samples. This may be the reason why the hysteresis loops changed from the H1 type of mesoporous silica to the H2 type of OMCs in the N_2 adsorption–desorption isotherms, as shown in Fig. S7 and Fig. 1(b), respectively. In addition, when the carbonization temperature increased, the walls of the mesoporous channels were more ordered and stable. This is in good agreement with the XRD data of Fig. 1(a) that demonstrates that increasing the carbonization temperature leads to an increase in the level of order in the mesoporous structure.

Scheme 1 summarizes the synthesis process of well-ordered mesoporous carbon materials. In particular, FA first filled the pores of the mesoporous silica templates. After carbonization at a high temperature, FA changed to carbon materials inside the mesopores of silica templates. The void spaces, which were generated by dissolving the silica templates in NaOH solution, become the mesopores of the OMCs. Consequently, CMK-3-*x* and CMK-8-*x* present similar pore structures to those of SBA-15 and KIT-6, respectively. The size of the mesopores (2–50 nm) is much larger than the size of the electrolyte ions. Therefore, ClO_4^- ions can be adsorbed-desorbed in the easy and fast ways to/from OMCs via the mesoporous channels, as shown in Scheme 1. The mesopores of OMCs provide not only fast pathway for ion transport but also the active sites for ion adsorption–desorption. A higher specific surface area leads to faster ion diffusion and a higher pore volume results in larger numbers of active sites for ion containment. This means that OMCs with a higher specific surface area and mesopore volume may present better EDLC performance.

3.2. Electrochemical performance of OMCs

Fig. 3(a) and (b) show the cyclic voltammogram (CV) curves of CMK-3-*x* and CMK-8-*x* synthesized at different carbonization temperatures. The broad rectangular shape of the CV curves reveals the double-layer capacitive behavior of the OMCs [38]. The shape profile of the CV curves and the output current of the CV curves drastically change with the mesoporous structure and synthesis temperature of CMK-3-*x* and CMK-8-*x*. Increasing the carbonization temperature of both CMK-3-*x* and CMK-8-*x* greatly increases the output current of the EDLCs, indicating the enhanced adsorption–desorption behavior and specific capacitance of OMCs synthesized at higher carbonization temperatures. Based on the area retained under the CV curves, the CMK-3-*x* electrodes exhibit a larger output-current response than CMK-8-*x*, demonstrating the better EDLC performance of CMK-3-*x* compared to CMK-8-*x*.

Fig. 3(c) and (d) demonstrate the charge–discharge curves of EDLCs in a potential range of 0–3 V at a current density of 0.2 A g^{-1}. The symmetric triangular charge–discharge curves reveal the appearance of a non-faradic and surface adsorption reaction during the charge–discharge process. It can be clearly noted that

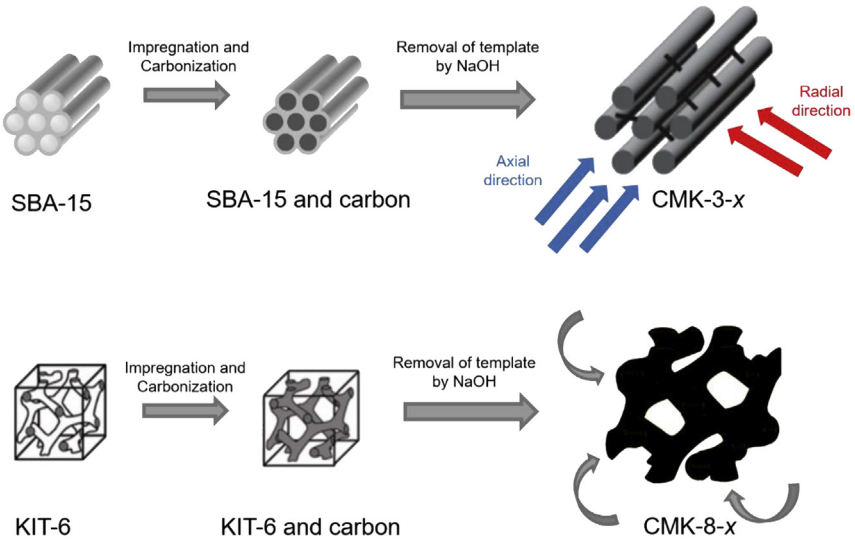

Scheme 1. Preparation processes of well-ordered mesoporous carbon materials.

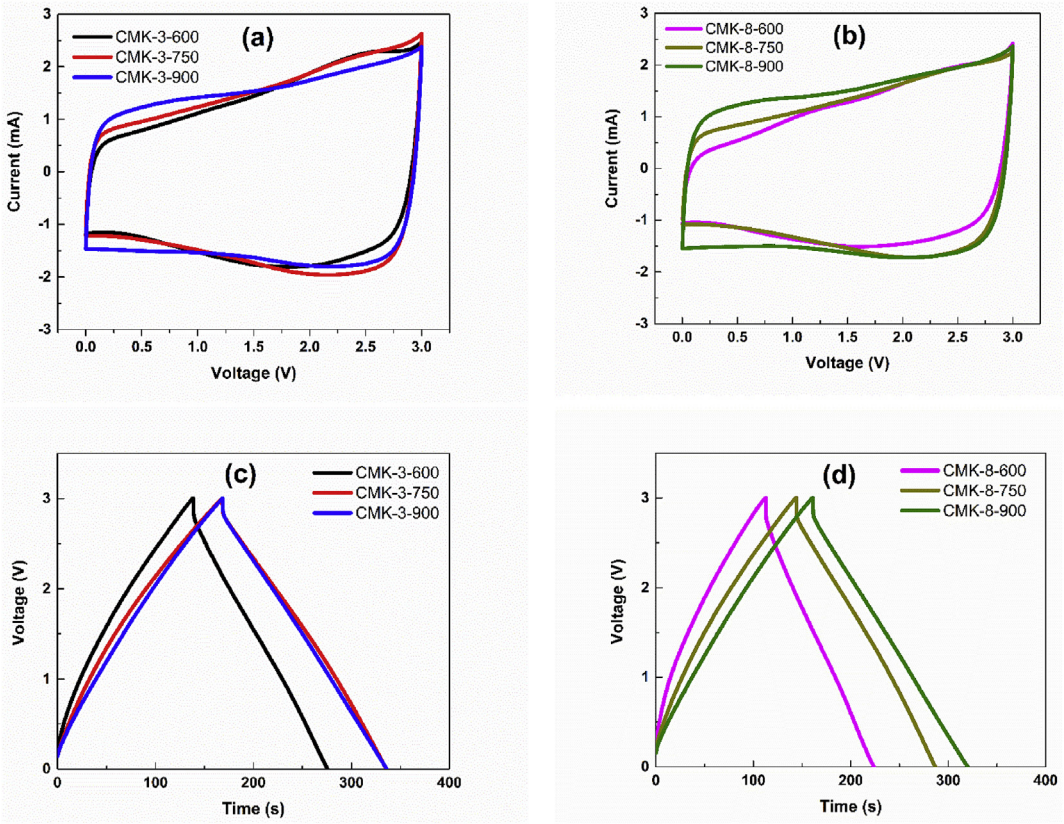

Fig. 3. (a) Cyclic voltammetry curves at a scan rate of 10 mV s^{-1} and (b) galvanostatic charge–discharge curves at 0.2 A g^{-1} of CMK-3-*x* samples. (c) Cyclic voltammetry curves at a scan rate of 10 mV s^{-1} and (d) galvanostatic charge–discharge curves at 0.2 A g^{-1} of CMK-8-*x* samples.

increasing the carbonization temperature increases the discharge time of both CMK-3-*x* and CMK-8-*x*. CMK-3-*x*-based cells achieved a longer discharge time compared to CMK-8-*x*-based cells. Among these samples, CMK-3-900 exhibits the longest discharge time, depicting the largest specific capacitance. The increase in the capacitance of OMCs with increasing carbonization temperature is attributed to the increase in the mesoporous surface area of the OMCs. The increase in the average pore size and mesoporous surface area of CMK-3-900 and CMK-8-900 can provide a large number of effective pores for large ions from non-aqueous electrolytes, which is also beneficial for ion diffusion and storage [16,39]. The higher discharge time of CMK-3-900 than CMK-8-900 originates from the ordered pore channels in CMK-3-900, which favors rapid ion-transfer kinetics more so than the cubic channels of CMK-8-900.

Nyquist impedance spectroscopy was utilized to further

understand the electrochemical properties of the OMCs, and the results are shown in Fig. 4. The Nyquist plots show a semicircle in the high-frequency Warburg region and a highly variable messy line in the low-frequency region, ascribed to charge-transfer reactions and transportation of electrolyte ions into the pores of carbon electrodes, respectively [40,41]. The decreasing semicircle with increasing carbonization temperature suggests a lower internal resistance for ion transport. This may come from the larger pore size of the OMCs carbonized at a higher temperature, which leads to the rapid diffusion of electrolyte ions. Moreover, the long straight channels of CMK-3-*x* provide a short diffusion pathway for electrolyte ions to arrive rapidly inside the mesopores than CMK-8-*x*, thus exhibiting a lower internal resistance.

Fig. 5 shows the cyclic stability of OMCs performed at a current density of 2.5 A g^{-1} for 10,000 cycles. All of the OMCs can remain the specific capacitance even after 10,000 charge–discharge cycles, indicating excellent cyclic stability (approximately 90%). CMK-3-*x* and CMK-8-*x* showed higher specific capacitance than MC-*x* due to the mesoporous nature of the former. MC-*x*, which has no mesopores, delivers a low capacitance (<20 F g^{-1}), indicating that the presence of mesopores enhances the specific capacitance of a given material. The micropores inside the MC-*x* samples are so small that the diffusion speed of electrolyte ions (ClO_4^-) can be very slow during the charge–discharge process. The low surface area and slow diffusion induced by small pore size of MC-*x* leads to the low specific capacitances, especially at a high loading-current density [42]. In contrast, the mesoporous structures of CMK-3-*x* and CMK-8-*x* provide not only a high specific surface area, increasing the ion storage, but also the large pores are beneficial for ion-diffusion pathways [15,43]. J. M. Rojo et al. investigated the influence of pore size on EDLC performance and revealed that the mesopores contribute to the specific capacitance much more than micropores [44]. This is in good agreement with G. Zhang et al. who found that the mesoporous structure is a suitable architecture for use in EDLCs for high capacitance and long cycle life [45].

In the case of OMCs, the CMK-3-*x* samples exhibit higher specific capacitance than CMK-8-*x* samples, which can be attributed to the difference in the pore structure between CMK-3-*x* and CMK-8-*x*. The electrolyte ions can easily diffuse into the mesopores of CMK-3-*x* not only along the straight channels (axial direction) but also from the other sides into the channels (radial direction), as displayed in Scheme 1. This forms a larger number of ion-transport pathways than that of *Ia3d* cubic CMK-8-*x* with closely packed and entangled channels. As a consequence, CMK-3-*x* materials exhibit faster ion transport and better EDLC performance than CMK-8-*x* samples. It also indicates that the mesoporous structure plays a crucial role in the EDLC performance of carbon-based electrodes.

In addition to the influence of the mesoporous structure, the effect of the specific surface area of carbon materials on EDLC performance was also studied. Fig. 6(a) displays the relationship between the BET specific surface area (S_{BET}) and the specific capacitance of CMK-3-*x* and CMK-8-*x*. It can be observed that there is no clear correction between S_{BET} and the specific capacitance. When the carbonization temperature increases from 600 to 900 °C, the specific capacitance of CMK-3-*x* and CMK-8-*x* increased from 55 to 78 F g^{-1} and from 35 to 66 F g^{-1}, respectively, by a factor of approximately 1.5. However, S_{BET} of CMK-3-*x* slightly increased from 859.7 (CMK-3-600) to 1064 (CMK-3-900) m^2 g^{-1}, whereas S_{BET} of CMK-8-*x* samples are similar (~950 m^2 g^{-1}), as shown in Table 1. This indicates that the increase in the specific capacitance cannot be explained by the change in BET specific surface area and that other variables with physical meaning should be found.

Fig. 6(b) displays the correlation between the mesoporous surface area of a series of carbon samples (CMK-3-*x* and CMK-8-*x*) and the specific capacitance. The mesoporous surface areas were obtained by the *t-plot* method. CMK-3-*x* and CMK-8-*x* materials

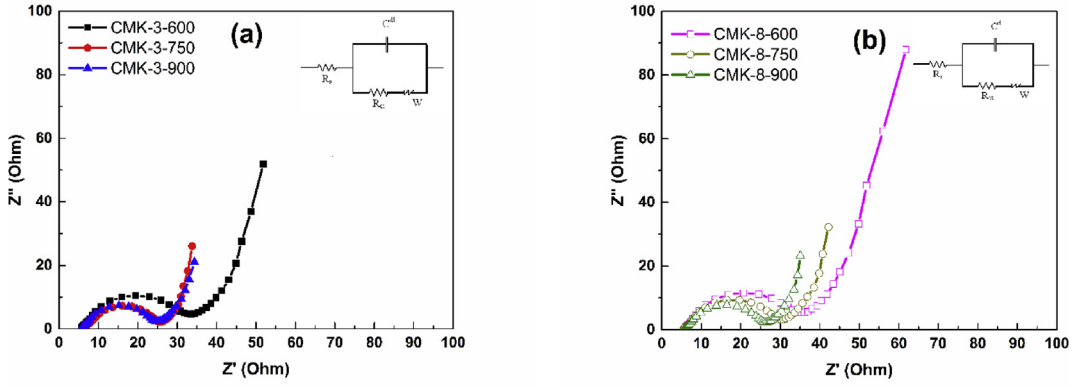

Fig. 4. Nyquist plots of (a) CMK-3-*x* samples and (b) CMK-8-*x* samples.

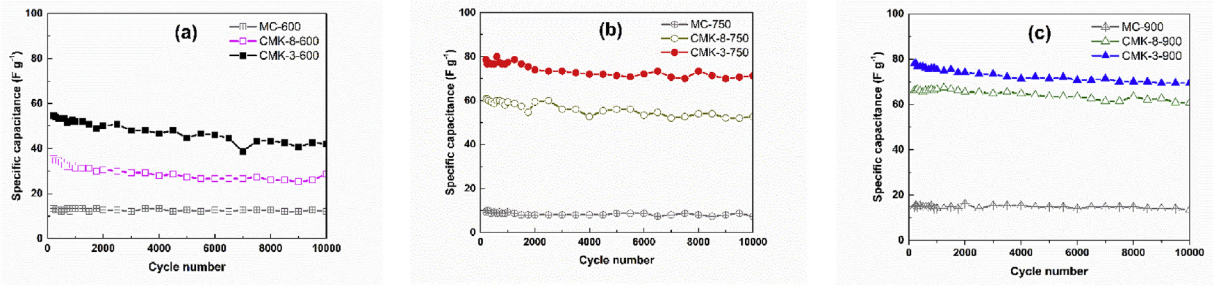

Fig. 5. Cyclic stability of different carbon electrodes at a current density of 2.5 A g^{-1}.

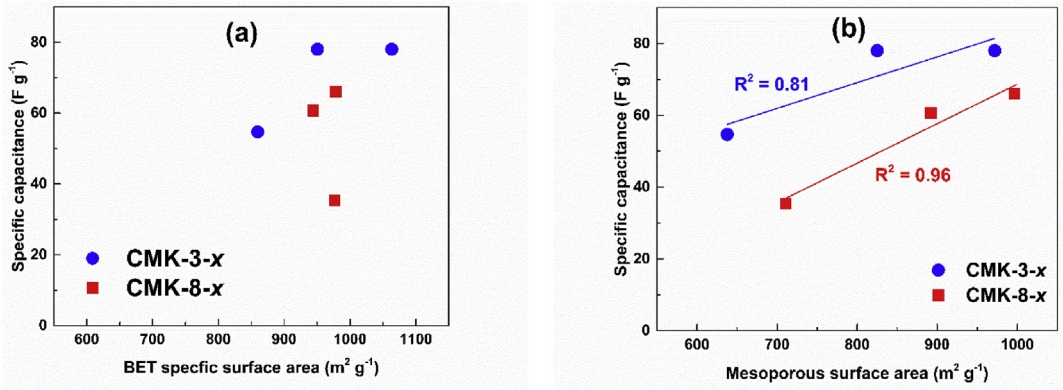

Fig. 6. Correlation between (a) BET specific surface area, (b) mesopore surface area, and the corresponding specific capacitance.

exhibit ideal linear relationships between the mesoporous surface area and the specific capacitance with high R^2 values (0.81 and 0.96, respectively). This means that the double-layer capacitance of OMCs employing non-aqueous electrolytes are governed by the mesoporous surface area of the OMCs because the large electrolyte ions are easily able to access the mesopores and not the micropores. The MC-*x* samples with microporous structures have low capacitance, as they did not have effective pores and surface area for access by electrolyte ions. Micropores are not suitable for the fast diffusion and immediate storage of electrolyte ions. Thus, the surface area of micropores may not contribute to the increase in specific capacitance in our experiments. Only mesopores with a larger size than that of electrolyte ions are accessible for the fast transportation of electrolyte ions in the charge–discharge process. With the increasing carbonization temperature from 600 to 900 °C, the mesoporous surface areas of CMK-3-*x* and CMK-8-*x* increase, which leads to the enhancement of the specific capacitance. It also means that the surface area of the mesopores in the CMK-3-*x* and CMK-8-*x* samples plays an important role in the EDLC performance.

4. Conclusions

The pores of the well-ordered mesoporous carbon materials synthesized from mesoporous silica (SBA-15 and KIT-6) templates are engineered to study the performance of EDLCs employing non-aqueous electrolytes. The study shows that the carbonization temperature strongly affects the pore properties of the OMCs, which in turn greatly influence the adsorption kinetics of OMCs. The long straight channels of CMK-3-*x* (prepared using SBA-15) show superior performance to that of CMK-8-*x* (prepared using KIT-6) with cubic channels. In EDLCs, highly porous OMCs with larger surface areas and larger pore volumes exhibit better performance than OMCs without mesopores. Moreover, the study reveals that the specific capacitance of EDLCs depends on the mesoporous surface area (S_{meso}) rather than the BET specific surface area (S_{BET}). The mesopores, with pore sizes larger than the electrolyte ion size, facilitate fast ion transportation and low internal resistance, leading to a higher specific capacitance. CMK-3 carbonized at 900 °C delivered the highest capacitance and good stability (~90% retention after 10,000 cycles at 2.5 A g^{-1}), outperforming the other samples.

Acknowledgement

This work was supported by the National Research Foundation of Korea (NRF) grant funded by the Korea government (Ministry of Science, ICT and Future Planning) (No. 2016R1A4A1012224).

Appendix A. Supplementary data

Supplementary data to this article can be found online at https://doi.org/10.1016/j.jallcom.2018.11.348.

References

[1] B. Dunn, H. Kamath, J.M. Tarascon, Electrical energy storage for the grid: a battery of choices, Science 334 (2011) 928–935.
[2] A.L.M. Reddy, S.R. Gowda, M.M. Shaijumon, P.M. Ajayan, Hybrid nanostructures for energy storage applications, Adv. Mater. 24 (2012) 5045–5064.
[3] M.V. Reddy, G.V.S. Rao, B.V.R. Chowdari, Metal oxides and oxysalts as anode materials for Li ion batteries, Chem. Rev. 113 (2013) 5364–5457.
[4] A. Manthiram, Y. Fu, S.H. Chung, C. Zu, Y.S. Su, Rechargeable lithium–sulfur batteries, Chem. Rev. 114 (2014) 11751–11787.
[5] N. Yabuuchi, K. Kubota, M. Dahbi, S. Komaba, Research development on sodium-ion batteries, Chem. Rev. 114 (2014) 11636–11682.
[6] L. Zhang, X. Hu, Z. Wang, F. Sun, D.G. Dorrell, A review of supercapacitor modeling, estimation, and applications: a control/management perspective, Renew. Sustain. Energy Rev. 81 (2018) 1868–1878.
[7] L. Mai, X. Tian, X. Xu, L. Chang, L. Xu, Nanowire electrodes for electrochemical energy storage devices, Chem. Rev. 114 (2014) 11828–11862.
[8] G. Wang, L. Zhang, J. Zhang, A review of electrode materials for electrochemical supercapacitors, Chem. Soc. Rev. 41 (2012) 797–828.
[9] D.S. Jeong, J.M. Yun, K.H. Kim, Highly porous nitrogen-doped carbon for superior electric double-layer capacitors, RSC Adv. 7 (2017) 44735–44742.
[10] G. Yu, X. Xie, L. Pan, Z. Bao, Y. Cui, Hybrid nanostructured materials for high-performance electrochemical capacitors, Nano Energy 2 (2013) 213–234.
[11] M. Vangari, T. Pryor, L. Jiang, Supercapacitors: review of materials and fabrication methods, J. Energy Eng. 139 (2013) 72–79.
[12] G.Z. Chen, Supercapacitor and supercapattery as emerging electrochemical energy stores, Int. Mater. Rev. 62 (2017) 173–202.
[13] C. Zhao, W. Zheng, A review for aqueous electrochemical supercapacitors, Front. Energy Res. 3 (2015) 23–33.
[14] L. Chang, W. Wei, K. Sun, Y.H. Hu, Excellent performance of highly conductive porous Na-embedded carbon nanowalls for electric double-layer capacitors with a wide operating temperature range, J. Mater. Chem. A 5 (2017) 9090–9096.
[15] X. Du, L. Wang, W. Zhao, Y. Wang, T. Qi, C.M. Li, Preparation of hierarchical porous carbon from waste printed circuit boards for high performance electric double-layer capacitors, J. Power Sources 323 (2016) 166–173.
[16] W. Li, D. Chen, Z. Li, Y. Shi, Y. Wan, G. Wang, Z. Jiang, D. Zhao, Nitrogen-containing carbon spheres with very large uniform mesopores: the superior electrode materials for EDLC in organic electrolyte, Carbon 45 (2007) 1757–1763.
[17] R. Yan, T. Heil, V. Presser, R. Walczak, M. Antonietti, M. Oschatz, Ordered mesoporous carbons with high micropore content and tunable structure prepared by combined hard and salt templating as electrode materials in electric double-layer capacitors, Adv. Sustain. Syst. 2 (2018) 1700128–1700139.
[18] K.L. Yang, S. Yiacoumi, C. Tsouris, Electrosorption capacitance of nanostructured carbon aerogel obtained by cyclic voltammetry, J. Electroanal. Chem. 540 (2003) 159–167.
[19] M. Karthik, E. Redondo, E. Goikolea, V. Roddatis, S. Doppiu, R. Mysyk, Effect of mesopore ordering in otherwise similar micro/mesoporous carbons on the high-rate performance of electric double-layer capacitors, J. Phys. Chem. C 118 (2014) 27715–27720.
[20] G.A. Ferrero, A.B. Fuertes, M. Sevilla, N-doped porous carbon capsules with tunable porosity for high-performance supercapacitors, J. Mater. Chem. A 3 (2015) 2914–2923.

[21] A. Borenstien, M. Noked, S. Okashy, D. Aurbach, Composite carbon nano-tubes (CNT)/Activated carbon electrodes for non-aqueous super capacitors using organic electrolyte solutions batteries and energy storage, J. Electrochem. Soc. 160 (2013) A1282–A1285.
[22] J.K. Mcdonough, A.I. Frolov, V. Presser, J. Niu, C.H. Miller, T. Ubieto, M.V. Fedorov, Y. Gogotsi, Influence of the structure of carbon onions on their electrochemical performance in supercapacitor electrodes, Carbon 50 (2011) 3298–3309.
[23] A. Daraghmeh, S. Hussain, I. Saadeddin, L. Servera, E. Xuriguera, A. Cornet, A. Cirera, A study of carbon nanofibers and active carbon as symmetric supercapacitor in aqueous electrolyte: a comparative study, Nanoscale Res. Lett. 12 (2017) 639–648.
[24] J.S. Moon, H. Kim, D.C. Lee, J.T. Lee, G. Yushin, Increasing capacitance of zeolite-templated carbons in electric double layer capacitors batteries and energy storage, J. Electrochem. Soc. 162 (2015) A5070–A5076.
[25] J.A. Fernández, M. Arulepp, J. Leis, F. Stoeckli, T.A. Centeno, EDLC performance of carbide-derived carbons in aprotic and acidic electrolytes, Electrochim. Acta 53 (2008) 7111–7116.
[26] T.N. Phan, M.K. Gong, R. Thangavel, Y.S. Lee, C.H. Ko, Ordered mesoporous carbon CMK-8 cathodes for high-power and long-cycle life sodium hybrid capacitors, J. Alloys Compd. 743 (2018) 639–645.
[27] A. Borenstein, O. Hanna, R. Attias, S. Luski, T. Brousse, D. Aurbach, Carbon-based composite materials for supercapacitor electrodes: a reviews, J. Mater. Chem. A 5 (2017) 12653–12672.
[28] J.S. Wei, S. Wan, P. Zhang, H. Ding, X.B. Chen, H.M. Xiong, S. Gao, X. Wei, Preparation of porous carbon electrodes from semen cassia for high-performance electric double-layer capacitors, New J. Chem. 42 (2018) 6763–6769.
[29] M. Kruk, M. Jaroniec, C.H. Ko, R. Ryoo, Characterization of the porous structure of SBA-15, Chem. Mater. 12 (2000) 1961–1968.
[30] S. Jun, S.H. Joo, R. Ryoo, M. Kruk, M. Jaroniec, Z. Liu, T. Ohsuna, O. Terasaki, Synthesis of new, nanoporous carbon with hexagonally ordered mesostructure, J. Am. Chem. Soc. 12 (2000) 10712–10713.
[31] M. Lezanska, J. Wloch, G. Szymanski, I. Szpakowska, J. Kornatowski, Properties of CMK-8 carbon replicas obtained from KIT-6 and pyrrole at various contents of ferric catalyst, Catal. Today 150 (2010) 77–83.
[32] M. Kruk, M. Jaroniec, Gas adsorption characterization of ordered organic-inorganic nanocomposite materials, Chem. Mater. 13 (2001) 3169–3183.
[33] P. Schneider, Adsorption isotherms of microporous-mesoporous solids revisited, Appl. Catal. A Gen. 129 (1995) 157–165.
[34] A. Galarneau, F. Villemot, J. Rodriguez, F. Fajula, B. Coasne, Validity of the *t-plot* method to assess microporosity in hierarchical micro/mesoporous materials, Langmuir 30 (2014) 13266–13274.
[35] M.E. Casco, F. Badazewski, S. Gratz, A. Tolosa, V. Presser, B.M. Smarsly, L. Borchardt, Mechanochemical synthesis of porous carbon at room temperature with a highly ordered sp2 microstructure, Carbon 139 (2018) 325–333.
[36] L. Zhou, D. Liu, J. Li, H. Tang, Z. Xie, D. Qu, Electrochemical hydrogen storage in a nitrogen-doped uniformed microporous carbon, Int. J. Hydrogen Energy 43 (2018) 14096–14102.
[37] S. Heeg, L. Shi, T. Pichler, L. Novotny, Raman resonance profile of an individual confined long linear carbon chain, Carbon 139 (2018) 581–585.
[38] M. Kim, I. Oh, J. Kim, Superior electric double layer capacitors using micro- and mesoporous silicon carbide sphere, J. Mater. Chem. A 3 (2015) 3944–3951.
[39] M. Wu, P. Ai, M. Tan, B. Jiang, Y. Li, J. Zheng, W. Wu, Z. Li, Q. Zhang, X. He, Synthesis of starch-derived mesoporous carbon for electric double layer capacitor, Chem. Eng. J. 245 (2014) 166–172.
[40] A.A. Moya, Identification of characteristic time constants in the initial dynamic response of electric double layer capacitors from high-frequency electrochemical impedance, J. Power Sources 397 (2018) 124–133.
[41] Y. Wu, J.P. Cao, X.Y. Zhao, Z.Q. Hao, Q.Q. Zhuang, J.S. Zhu, X.Y. Wang, X.Y. Wei, Preparation of porous carbons by hydrothermal carbonization and KOH activation of lignite and their performance for electric double layer capacitor, Electrochim. Acta 252 (2017) 397–407.
[42] Z.Q. Hao, J.P. Cao, Y. Wu, X.Y. Zhao, Q.Q. Zhuang, X.Y. Wang, X.Y. Wei, Preparation of porous carbon sphere from waste sugar solution for electric double-layer capacitor, J. Power Sources 361 (2017) 249–258.
[43] Q. Li, R. Jiang, Y. Dou, Z. Wu, T. Huang, D. Feng, J. Yang, A. Yu, D. Zhao, Synthesis of mesoporous carbon spheres with a hierarchical pore structure for the electrochemical double-layer capacitor, Carbon 49 (2011) 1248–1257.
[44] A.B. Fuertes, F. Pico, J.M. Rojo, Influence of pore structure on electric double-layer capacitance of template mesoporous carbons, J. Power Sources 133 (2004) 329–336.
[45] C. Li, X. Yang, G. Zhang, Mesopore-dominant activated carbon aerogels with high surface area for electric double-layer capacitor application, Mater. Lett. 161 (2015) 538–541.